Optimized tin-doped and undoped zinc oxide thin layers for photovoltaic application

RAZIKA TALA-IGHIL[a,b], FAYÇAL BENSOUICI[b], BILEL LARAB[b], SAMIR BACHIR[b], MAHDIA TOUBANE[b], DJEDJIGA HAOUANOH[b], AICHA IRATNI[b]

[a]*Institute of Electrical & Electronic Engineering, Université M'hamed Bougara Boumerdes, Rue de l'Indépendance, Boumerdes 35000, Algeria*
[b]*Unité de Recherche des Matériaux, des Procédés et Environnement, Université M'hamed Bougara Boumerdes, Rue de l'Indépendance, Boumerdes 35000, Algeria*

The present work focuses on the structural and optical properties study of undoped zinc oxide ZnO and tin-doped zinc oxide ZnO:Sn thin films deposited by the spray pyrolysis technique. Variations of zinc acetate concentration and substrate temperature have been made. Two concentrations and two substrate temperatures values have been adopted: 0.4 mol/l, 0.5 mol/l and 400°C, 500°C, respectively. Doped zinc oxide layers have been realized by adding tin tetrachloride ($SnCl_4$) in the sprayed solution. The films were characterized by X-ray diffraction (XRD) and UV-visible spectroscopy to determine their structural and optical properties. For the 0.4mol/l zinc acetate precursor concentration, a high crystallinity for the doped layers is noticed compared to the undoped ones, while in the case of 0.5 mol/l zinc acetate, the opposite behaviour is remarked, between the doped and the undoped layers. By analyzing the transmission and reflection spectra, it was found that zinc oxide energy gap shifts to lower values with tin doping and with substrate temperature increase. It is enhanced with precursor concentration rise.

1. Introduction

Transparent conducting oxides (TCO's) are, in general, semiconductors characterized by their good electrical conductivity and high transparency in the visible spectrum. They play the role of front electrode and window layer in solar cells [1]. Most common TCO's used are tin dioxide (SnO_2), indium tin oxide (ITO) and zinc oxide ZnO. Zinc oxide layers have a wide range of applications thanks to their non-toxicity and low cost [2-4].

The main challenge in the photovoltaic energy consists in reducing the solar cell cost. Thus, the use of the deposition technique is critical. We must choose the technique that requires less energy bill and which not need vacuum (unlike the sputtering technique for example). It must also allow the deposition on large substrates' surfaces in addition to the deposition time which not exceed few minutes [5-6]. The most suitable one is spray pyrolysis technique compatible for large scale solar cells fabrication despite the fact of defects presence disadvantage in the open environment. The latter inconvenient can be reduced by working in a clean room.

It is well-known that stoichiometric ZnO is not stable due to thermodynamic reasons at room temperature and pressure. In addition to the fact that oxygen vacancies are generally present in ZnO [7]. For this purpose, ZnO thin films doping is used to increase their electrical conductivity [7]. For example, Mn-doped ZnO thin layers let them behave like diluted magnetic semiconductors used in spintronics [8, 9] while Al doped ZnO was widely studied for gas sensors [10] and for solar cells [5].

The present paper focuses on the properties of Sn-doped ZnO layers as front electrode in photovoltaic cell. Doping with tin atoms has been performed because Sn becomes Sn^{+4} when it replaces Zn^{+2} site in the ZnO crystal structure, providing two additional electrons those contribute to conduction. Knowing that the crystal ionic radius of Zn^{+2} (88pm) and Sn^{+4} (83pm) is nearly the same, it is clear that the possible Zn^{+2} substitution by Sn^{+4} would be accompanied by a slight lattice contraction. Additionally, it is very important to mention that according the well-known Hume–Rothery rules [11], the ionic radius difference should be less than 15%, which is the case here. Highly degenerate fluorine doped tin oxide SnO_2:F is also a good front electrode TCO deposited by spray pyrolysis for a solar cell but it has the incovenient of HCl emanation during the deposition process [12]. With our ZnO:Sn, we combine the good electrical properties coming from tin doping with an healthy friendly material ZnO. We ensure also the layer stability.

The tin doped zinc oxide has proven its effect for enhancing the electrical and optical properties [13] A solar-to-electricity conversion efficiency of ~1.82% is achieved by DSSC (Dye sensitized solar cell (DSSC)) fabricated with Sn-ZnO photoanode, while the relatively low conversion efficiency of ~1.49% is attained by DSSC with ZnO photoanode. The superior photovoltaic performance might attribute to the significant Sn-ion doping ZnO nanostructures which might improve the high

charge collection and the transfer of electrons at the interfaces of doped ZnO layer and the electrolyte layer [14].

The work originality consists in Sn doping effect on ZnO layers deposited by spray pyrolysis technique and starting from zinc acetate and tin chloride for a specific application as highly degenerate front electrode (window layer) for the solar cells. The difference compared to the work of M. Ajili et al. [15] is the sprayed solution composition and the layer thickness. Many investigations have been performed with other techniques [16].

2. Experimental details

Silicon samples undergo all the steps of the chemical cleaning, in order to be ready for spray pyrolysis deposition [17-19]. The home made spray pyrolysis experimental set up is shown in Fig. 1, below:
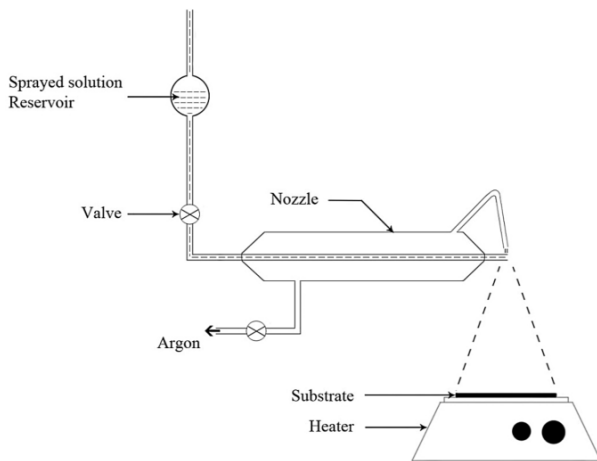
Fig. 1. Spray pyrolysis set-up

Zinc acetate is dissolved in a mixture containing methanol and deionized water with proportions 3:1. Few drops of acetic acid are added to permit the total zinc acetate dissolution in the solution. Finally, a white transparent solution with concentration 0.4 mol/l and 0.5mol/l is obtained. Doped zinc oxide layers have been prepared by adding $SnCl_4$ in the sprayed solution.

Doping is obtained by adding $SnCl_4{:}5H_2O$ by respecting [Sn]/[Zn] = 3at%.

The studied interval for zinc acetate concentration (0.4 mol/l and 0.5 mol/l only) is not too large because it is an interval around the optimum value; the other concentrations didn't give us significant results for the optical and structural properties.

Argon is first applied and then the zinc acetate based mixture is sprayed onto the heated silicon substrates.

The spary pyrolysis technique has been adopted to deposit the ZnO and Sn doped ZnO thin films (Fig. 1). The substrate temperature sweep from 400°C to 500°C and the distance nozzle-substrate is 30cm. The thickness of all samples is kept constant and is equal to 80 nm and is controlled by the spraying time. It is the optimum

thickness for transparent conducting oxides TCO window layers. Experimentally, this thickness is observed by naked eye with the color royal blue on silicon substrates and is confirmed with ellipsometry measures. It is also confirmed by the work of S. Rahmane et al. [23].

X-Ray diffraction spectra were obtained by using a Bruker D8 Advance diffractometer at normal incident with CuKα radiations (λ= 1.5418 Å). X-ray diffraction spectra of all the films were taken at room temperature.

The planes in a crystalline structure are identified by a series of integers called the Miller indices deduced as follow:
1. Crystal x,y,z axes definition.
2. Find the plane's intercepts along these axes.
3. Calculate the reciprocal of the intercepts and reduce them to the smallest integers (hkl) that represent a family of parallel and equivalent planes [21].

In order to explore the structural characterization, a non-destructive technique, X-Ray diffraction, is used. XRD spectrum contains a series of peaks in which peak intensity is plotted on the y-axis and diffraction angle (2θ) along the x-axis. Each peak corresponds to a set of planes (hkl) in the material [22]. It follows the well-known Bragg formula [23]:

$$2d_{hkl}\,sin\theta = n\lambda \qquad (1)$$

with: d_{hkl}: distance between two adjacent planes (hkl)
λ: X-Ray wavelength
θ: incident angle
n: diffraction order

Experimental spectra are compared with Joint Council Powder Diffraction (JCPDS) data for standards.

Optical transmittance and reflectance spectral were measured at normal incidence in UV–VIS–NIR spectral region (300–2500 nm) with a Varian Cary 500 Spectrophotometer.

3. Results and discussions

The obtained X-Ray diffraction spectra are shown in Figs. 2 and 3, below:
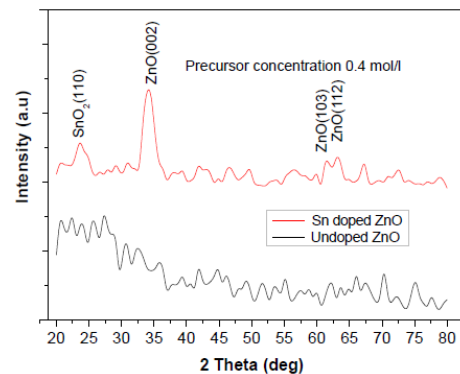
Fig. 2. X-Ray diffraction spectra for ZnO thin layers with precursor concentration 0.4 mol/l (a) ZnO:Sn, (b) undoped ZnO deposited onto silicon substrates at 500°C
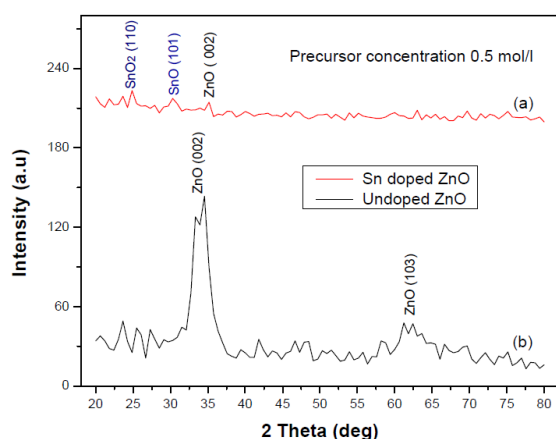
Fig. 3. X-Ray diffraction spectra for ZnO thin layers with precursor concentration 0.5 mol/l (a) ZnO:Sn, (b) undoped ZnO deposited onto silicon substrates at 500°C

Fig. 2 showed X-Ray diffraction spectra of ZnO thin films prepared with zinc acetate precursor concentration 0.4 mol/l. We can observe in Fig. 2a for the doped films with 0.4 mol/l precursor concentration three main peaks for 2θ at 34.422°, 62.864° and 67.963° corresponding to (002), (103) and (112) ZnO planes, respectively, according to the reference diffraction curve obtained for pure ZnO by the American Society for Testing and Material JCPDS 36-1451. The remaining peak at 26° corresponding to the SnO_2 (110) plane following JCPDS 01-0625 data. The Fig. 2b for the undoped layers, show no high cristallinity and the structure seems to be amorphous. Other authors also observed that Sn doped ZnO thin films have (002) as preferred orientation [24] and reported that the peak's intensity for the Sn doped ZnO films was higher than the one of the undoped and Sn doped ZnO thin films having (002) as preferred orientation.

According to ref [24], the incorporation of tin atoms in the ZnO structure don't affect the preferred orientation which is (002). This can be explained by the fact that Sn^{+4} will replace oxygen positions in the ZnO lattice. This permit to partially cure the crystal network and reinforce the intensity of (002) preferred orientation.

Fig. 3 showed the XRD spectra of 0.5 mol/l zinc acetate precursor concentration deposited at 500°C substrate temperature. Fig. (3.b) revealed a high cristallinity of the undoped ZnO thin films with the presence of two main peaks (002) and (103). While in Fig. (3.a) we can observe the presence of three phases: SnO_2, SnO (JCPDS N° 78-1913) and ZnO with corresponding peaks are (110), (101) and (002), respectively. The (002) peak intensity is reduced with doping. This remark is also found by V. R. Shinde et al. [25]. It is also noticed that the preferred orientation (002) shifts to higher diffraction angles. This result is consistent with the literature [16]. This shift to high angles can be explained by the ion dopant Sn^{+4} radius which is smaller than that of Zn^{+2} [26].

The structure for doped layers at 0.5 mol/l acetate concentration is just polycristalline. It may be explained by the presence of Sn atoms which act against plane (002) formation [26].

The Scherrer formula represents the relationship between the grain size and the broadening of the preferred orientation [27-28]

$$D = \frac{0.9\lambda}{FWHM \cos\theta} \qquad (2)$$

with D : grain size of the preferred orientation (hkl)

λ: wavelength of the incident X-rays CuKα (λ=1.5418 Å)

FWHM: full width at half maximum of the preferred orientation

θ: Diffraction angle

From the diffraction curves, the preferred orientation is the peak (002). This peak is observed for different dopants like ZnO:N [29]. After calculation, we conclude the following results summarized in Table 1:

Table 1. Grain size calculation for ZnO layers deposited from zinc acetate based sprayed solution with concentrations 0.5 mol/l and 0.4 mol/l

Preferred peak	2θ (°)	FWHM (°)	Intensity (a.u)	Grain size D (nm)
(002) Solution 0.5 mol/l	35	0.9375	145	15.58
(002) Solution 0.4 mol/l	34.422	1.97	100	4.227

Lattice parameters a and c determination:

As we know, zinc oxide layers crystallize in hexagonal wurtzite structure, the distance between (hkl) planes follow the formula below [30]:

$$d_{hkl} = \frac{1}{\frac{4}{3}\sqrt{(h^2+k^2+hk)+l^2\left(\frac{a^2}{c^2}\right)}} \qquad (3)$$

After replacing for (002), we found:

$d_{(002)}$= 2.03 Å and c= 5.4133 Å for the concentration 0.5 mol/l

$d_{(002)}$= 2.60 Å and c= 6.9333 Å for the concentration 0.4 mol/l

One can remarks the ZnO lattice structure compression with zinc acetate precursor concentration increase from 0.4 mol/l and 0.5 mol/l.
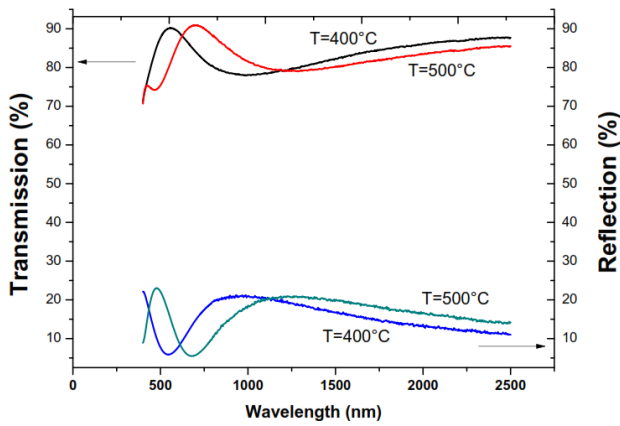
Fig. 4. Temperature effect onto optical properties of undoped ZnO layers deposited with precursor concentration at 0.5 mol/l
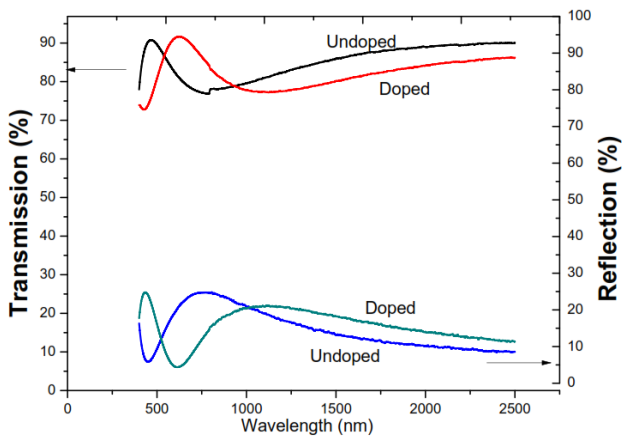
Fig. 5. Tin doping effect onto optical properties of ZnO layers deposited with precursor concentration at 0.4 mol/l at 450°C

The treatment of the previous optical curves obtained from spectrophotometry permit the absorption coefficient deduction according to the formula [31-32]:

$$\alpha(\lambda) = \frac{1}{d} \ln\left(\frac{1-R(\lambda)}{T(\lambda)}\right) \qquad (4)$$

With α(λ) : The layer absorption coefficient for the wavelength λ

d : The layer thickness

R(λ) : The layer reflection datum for the wavelength λ

T(λ) : The layer transmission datum for the wavelength λ

The plot of $(\alpha h\nu)^2$ versus energy allowed us to extract the energy gap for each sample.

The results are presented in Table 2 below:

Table 2. Energy gap for tin doped and undoped ZnO layers with precursor concentration 0.4 mol/l and 0.5 mol/l for substrate temperature range [400°C -500°C]

[Zn(CH₃COO)₂] precursor concentration (mol/l)	Doping with 3% Sn	Substrate temperature (°C)	Energy gap (eV)
0.4	Undoped	400	3.29
	Doped		3.27
	Undoped	450	3.29
	Doped		3.28
0.5	Undoped	400	3.31
	Undoped	450	3.29
	Doped		3.27
	Undoped	500	3.31
	Doped		3.30

The spectral optical transmittance T(λ) and reflectance R(λ) were measured at normal incidence in UV–VIS–NIR spectral region 300–2500 nm. In Fig. 4 and 5, the spectra reveal low pronounced interference effects in the transparency region 300–2000 nm with sharp fall of transmittance at the band edge. The interferences nonappearance due the low thickness of the deposited films. We can noticed that all the deposited ZnO layers show high transparency in the visible range (The interval of work of solar cells) with transmission more than 90% and reflection less than 10% in both figures 4 and 5 shown above. The transmission maximum value and the reflection minimum value shift from the wavelength 539 nm at temperature deposition 400°C to 669 nm at temperature deposition 500°C for undoped ZnO thin films with 0.5 mol/l zinc acetate precursor presented in Fig. 4.

These maxima and minima shift from 451 nm to 605 nm with doping for zinc acetate concentration at 0.4 mol/l zinc acetate precursor in Fig. 5 with substrate temperature 450°C.

The precursor concentration effect translates the transmission maxima and reflection minima to higher wavelength values which predict that the energy gap should shift to lower energies.

According to the energy gap tabulated data, we can notice that the zinc oxide gap tends to shift to lower values with tin doping and with substrate temperature increase. While, by increasing zinc acetate precursor concentration, the energy gap increases also. The energy shift to lower energies with tin doping is also observed by many authors, especially by A. D. Acharya et al. [33]. This can be explained by the fact that when tin doping is operated, deep levels were created and consequently the optical bandgap is reduced [33-34]. This behavior occurs also with substrate temperature increase. It was also observed by M. Benhaliliba et al. [35] with undoped and In-doped zinc oxide.

When the precursor concentration zinc acetate increased, the energy gap increases also [35]. This means that more Zn^{+2} is inserted to the thin film layer. With the presence of doping element Sn^{+4}, the ZnO layer tends to choose its equilibrium state with Zn^{+2} rather than Sn^{+4}. The deep tin level states were reduced and lead to the energy gap increase [36]. N. Chahmat et al. have found an energy gap value equal to 3.26eV for Sn at %=4% [37]. This value is closest to ours 3.27eV with Sn at% = 3%.

4. Conclusion

Transparent undoped zinc oxide and tin doped zin oxide films have been successfully deposited by spray pyrolysis technique and studied. Tin doping has been carried out by adding few drops of $SnCl_4.5H_2O$ in the spraying mixture. The structural properties were investigated for both cases (undoped, ZnO:Sn) for two zinc acetate concentrations (0.4 mol/l) and (0.5 mol/l). For 0.5mol/l zinc acetate concentration, the (002) Miller peak represents the preferred orientation in undoped layers with a grain size of 15.58 nm and wurtzite lattice parameters a = 2.03 Å and c=5.41 Å and has a position 2θ = 34°. This position is shifted to higher angles 2θ = 35° after tin doping. This can be explained by the Sn^{+4} ion radius which is smaller than Zn^{+2} ion radius.

The peak (002) intensity decreases with doping because the tin Sn atoms present in the lattice forbid the growth of ZnO growth along (002). From this study, we can tune the ZnO:Sn energy gap. This is a main advantage to reduce the lattice mismatch between the window layer ZnO:Sn and the absorber layer. As we know that in solar cells, when the interface effects are mastered, we can get higher conversion efficiency. As a conclusion, the zinc oxide layers structural properties are directly linked to the sprayed solution concentration and to the doping atom nature.

References

[1] Claes G. Granqvist, Solar Energy Materials & Solar Cells **91**(17), 1529 (2007).
[2] S. Menakh, Magister thesis, Constantine (2010).
[3] Jamil Elias, PhD thesis, PARIS-XII (2008).
[4] Yangyang Zhang, College of Engineering, University of Florida, USA. April 2004.
[5] A. Nakaruk, C. C. Sorell, Journal of Coating Technology Research, **7**(5) 665 (2010).
[6] Dainius Perednis, Ludwig J. Gauckler, Journal of Electroceramics **14**(2), 103 (2005).
[7] Shalaka C. Navale, I. S. Mulla, Materials Science and Engineering C **29**(4), 1317 (2009).
[8] L. Yan, C. K. Ong, X. S. Rao, Journal of Applied Physics **96**(1), 508 (2004).
[9] R. Mimouni, O. Kamoun, A. Yumlak, A. Mhamdi, K. Boubaker, P. Petkova, M. Amlouk, Journal of Alloys and Compounds **645**, 100 (2015).
[10] B. Baruwati, D. K. Kumar, S. V. Manorama, Sensors & Actuators **B119**, 676 (2006).
[11] C. Kittel, Introduction to Solid State Physics, seventh ed., John Wiley & Sons, 614 (1996).
[12] R. Tala-Ighil, M. Boumaour, M. S. Belkaïd, A. Maallemi, K. Melhani, A. Iratni, Solar Energy Materials and Solar Cells **90**(12), 1797 (2006).
[13] M. Peiteado, Y. Iglesias, J. F. Fernandez, J. De Frutos, A. C. Caballero, Mater. Chem. Phys. **101**(1), 1 (2007).
[14] Sadia Ameen, M. Shaheer Akhtar, Hyung-Kee Seo, Young Soon Kima, Hyung Shik Shin, Chemical Engineering Journal **187**, 351 (2012).
[15] Mejda Ajili, Michel Castagné, Najoua Kamoun Turki, Sperlattices and Microstructures **53**, 213 (2013).

[16] Chien-Yie Tsay, Hua-Chi Cheng, Yen-Ting Tung, Wei-Hsing Tuan, Thin Solid Films **517**(3), 1032 (2008).
[17] S. A. Studenikin, N. Golego, M. Cocivera, Journal of Applied Physics **84**(4), 2287 (1998).
[18] C. Messaoudi, D. Sayah, M. Abd-Lefdil, Physica Status Solidi (A) Applied Research, 1995.
[19] A. Maldonado, M.de la Luz Olvera, S. Tirado Guerra, R. Asomoza, Solar Energy Materials & Solar Cells **82**(1-2), 75 (2004).
[20] S. Rahmane, M. S. Aida, M. A. Djouadi, N. Barreau, Superlattices and Microstructures **79**, 148 (2015).
[21] Umesh K. Mishra, Jasprit Singh, "Semiconductor device physics and design" p.9, Springer 2008; DOI: 10.1007/978-1-4020-6481-4.
[22] M. Birkholz, C. Genzel, T. Jung, Journal of Applied Physics **96**, 7202 (2004).
[23] Vardaan Chawla, PhD thesis, Stanford University, December 2011.
[24] A. Bougrine, A. El Hichou, M. Addou, J. Ebothé, A. Kachouane, M. Troyon, Materials Chemistry and Physics **80**, 438 (2003).
[25] V. R. Shine, T. P. Gutar, C. D. Lokhande, R. S. Mane, Sung-Hwan Han, Materials Chemistry and Physics **96**, 326 (2006).
[26] K. C. Park, D. Y. Ma, K. H. Kim, Thin Solid Films **305**, 201 (1997).
[27] F. D. Paraguay, W. L. Estrada, D. R. N. Acosta, E. Andrade, M. Miki-Yoshida, Thin Solid Films **350**(1-2), 192 (1999).
[28] A. Patterson, Physics Review **56**(10), 978 (1939).
[29] S. Majudar, S. Chat Topadhyay, P. Banerji, India Institute of Technology 2009.
[30] A. Mosbah, M. S. Aida, Journal of Alloys and Compounds **515**, 149 (2012).
[31] L. S. Roman, R. Valaski, C. D. Canestraro, E. S. C. Magallaes, C. Persson, R. Ahuja, E. F. da Silva Jr., I. Pepe, A. Ferreira da Silva, Applied Surface Science **252**(15), 5361 (2006).
[32] Yow-Jon Lin, Chia-Lung Tsai, Yang-Ming Lu, Chia-Jyi Liu, Journal of Applied Physics **99**(9), 0093501 (2006).
[33] A. D. Acharya, Shweta Moghe, Richa Panda, S. B. Shrivastava, Mohan Gangrade, T. T. Shripathi, D. M. Phase, V. Ganesan, Journal of Molecular Structure **1022**, 8 (2012).
[34] K. C. Yung, H. Liem, H. S. Choy, Journal of Physics D, Applied Physics **42**(18), 185002 (2009).
[35] H. Benhaliliba, C. E. Benouis, Z. Mouffak, Y. S. Ocak, A. Tiburcio-Silver, M. S. Aida, A. A. Garcia, A. Tavira, A. Sanchez Juarez, Superlattices and Microstructures **63**, 228 (2013).
[36] Bhavana N. Joshi, Hyun Yoon, Ho Young Kim, Joon Ho Oh, Tae Yo Seong, Scott C. James, Sam S. Yoon, Journal of Electrochemical Society **159**(8), H716 (2012).
[36] Nadia Chahmat, Ammar Haddad, Azzedine Ain-Souya, Rachid Ganfoudi, Nadir Attaf, Mouhamed Salah Aida, Mokhtar Ghers, Journal of Modern Physics **3**, 1781 (2012).

*Corresponding author: t_razika@hotmail.com